

Superconducting properties and Fermi-surface topology of the quasi-two-dimensional organic superconductor λ -(BETS) $_2$ GaCl $_4$.

Charles Mielke^{1,§}, John Singleton^{1,2}, Moon-Sun Nam², Neil Harrison¹, C.C. Agosta³, B. Fravel⁴ and L. K. Montgomery⁴

¹National High Magnetic Field Laboratory, Los Alamos National Laboratory, MS-E536, Los Alamos, New Mexico 87545, USA

²University of Oxford, Department of Physics, The Clarendon Laboratory, Parks Road, Oxford OX1 3PU, U.K.

³Department of Physics, Clark University, Worcester, MA 01610, USA

⁴Department of Chemistry, Indiana University, Bloomington, Indiana 47405, USA

Abstract. The Fermi surface topology of the organic superconductor λ -(BETS) $_2$ GaCl $_4$ has been determined using the Shubnikov-de Haas and magnetic breakdown effects and angle-dependent magnetoresistance oscillations. The former experiments were carried out in pulsed fields of up to 60 T, whereas the latter employed quasistatic fields of up to 30 T. All of these data show that the Fermi-surface topology of λ -(BETS) $_2$ GaCl $_4$ is very similar to that of the most heavily-studied organic superconductor, κ -(BEDT-TTF) $_2$ Cu(NCS) $_2$, except in one important respect; the interplane transfer integral in λ -(BETS) $_2$ GaCl $_4$ is a factor ~ 5 larger than that in κ -(BEDT-TTF) $_2$ Cu(NCS) $_2$. The increased three-dimensionality of λ -(BETS) $_2$ GaCl $_4$ is manifested in radiofrequency penetration-depth measurements, which show a clear dimensional crossover in the behaviour of $H_{c2}(T)$. The radiofrequency measurements have also been used to extract the Labusch parameter determining the fluxoid interactions as a function of temperature, and to map the flux-lattice melting curve.

Submitted to: *J. Phys.: Condens. Matter*

§ To whom correspondence should be addressed (cmielke@lanl.gov)

1. Introduction

There is considerable current debate over the nature of superconductivity in quasi-two-dimensional (Q2D) crystalline organic metals [1, 2, 3, 4]. The most heavily studied members of this family of materials are the κ -phase BEDT-TTF salts (e.g. κ -(BEDT-TTF) $_2$ Cu(NCS) $_2$) [1]. Whilst nuclear magnetic resonance [5], penetration-depth [2], tunnelling [4] and other experiments [1] appear to suggest that the superconductivity in these salts may be d-wave-like and mediated by spin-density-wave-like fluctuations, some doubts have been cast by recent controversial specific heat measurements, which may suggest that the order parameter does not possess the required nodes [3]. Several theories [6, 7, 8, 9] stress the importance of the details of the Fermi-surface topology in providing suitable prerequisites for superconductivity; if the Fermi-surface geometry and interactions are altered slightly, it appears that BCS-like s-wave superconductivity *may* be the dominant low-temperature groundstate [1].

Clearly, it is of importance to study organic superconductors with slight variations in Fermi-surface topology so that the effect on the superconducting groundstate can be assessed. In this paper we therefore report magnetotransport and radiofrequency penetration-depth measurements of the superconductor λ -(BETS) $_2$ GaCl $_4$. Shubnikov-de Haas oscillations, magnetic breakdown and angle-dependent magnetoresistance oscillations indicate that the effective masses of λ -(BETS) $_2$ GaCl $_4$ and much of the topology of its Fermi surface are similar to those of the most heavily-studied BEDT-TTF superconductor, κ -(BEDT-TTF) $_2$ Cu(NCS) $_2$. However, the magnetoresistance close to $\theta = 90^\circ$ implies that the interplane transfer integral in λ -(BETS) $_2$ GaCl $_4$ is approximately five times larger than that in κ -(BEDT-TTF) $_2$ Cu(NCS) $_2$, suggesting that λ -(BETS) $_2$ GaCl $_4$ is less two-dimensional. This increased dimensionality is manifested in the superconducting properties of λ -(BETS) $_2$ GaCl $_4$; a clear two-dimensional to three dimensional crossover is seen in the temperature dependence of H_{c2} . We have also used the radiofrequency measurements to extract various parameters related to the interactions between the fluxoids and to reveal the melting of the vortex solid.

2. Background information

When the innermost four sulphur atoms of BEDT-TTF [1] are replaced by selenium to produce BETS (where BETS stands for bis(ethylenedithio)tetraselenafulvalene), electrocrystallization gives rise to a range of charge-transfer salts with notably different properties compared to their BEDT-TTF counterparts [10, 11, 12, 13]. Salts of the λ -phase morphology are presently unique to the BETS series, and λ -(BETS) $_2$ GaCl $_4$ ($T_c \approx 5$ K) remains the only superconducting BETS charge-transfer salt found thus far [12, 14].

Crystals of the λ -phase exist in the form of needles with the long axis of the needle corresponding to the shortest lattice vector \mathbf{c} [11, 12]. At first sight, the crystal structure looks quasi-one-dimensional, with the BETS molecules packing roughly parallel in the planes between the anions [12]. However, the BETS sites are not equivalent,

and the cation molecules in fact occur in dimers, surrounded roughly isotropically by four nearest-neighbour dimers with the same orientation. The crystallographic unit cell contains two dimers, and hence contributes two holes [12]. Although the details of the cation positioning and symmetry are rather different than in κ -(BEDT-TTF) $_2$ Cu(NCS) $_2$ [1], the overall similarity of the dimer arrangements lead one to expect a Fermi surface for λ -(BETS) $_2$ GaCl $_4$ which is topologically similar to that in κ -(BEDT-TTF) $_2$ Cu(NCS) $_2$. Indeed, the calculated bandstructure of λ -(BETS) $_2$ GaCl $_4$ predicts a Fermi surface consisting of a quasi-two-dimensional (Q2D) hole pocket (the α pocket) and a pair of warped quasi-one-dimensional (Q1D) sheets [12, 15]. According to the calculations, the α pocket in this case is expected to occupy $\sim 28 - 33$ % of the Brillouin zone [12, 15].

3. Magnetotransport studies.

3.1. Experimental details.

Single crystals of approximately $1 \times 0.1 \times 0.05$ mm 3 were synthesized using electrochemical techniques [12] employing a 1,1,-trichloroethane/1,1,2-trichloroethane/ethanol solvent system [16]. For the purpose of performing four-wire resistance measurements, 12 μ m gold leads were attached to the samples using graphite paint. In the pulsed field experiments, the resistance was measured using a 10 μ A ac current with a frequency of 200 kHz [1, 17]. The voltage was measured using a high-speed lock-in amplifier. Temperatures as low as ~ 340 mK were achieved by immersing the sample in liquid 3 He inside a plastic cryostat [17]. Capacitor-driven, ~ 40 millisecond-duration pulsed magnetic fields of up to 60 T were provided by the National High Magnetic Field Laboratory (NHMFL), Los Alamos. Angle-dependent magnetoresistance (AMRO) studies were made using a two-axis rotation insert [1] in quasistatic magnetic fields of up to 30 T provided by NHMFL, Tallahassee. In the AMRO experiments, an ac current of 5 μ A (frequency 30 – 80 Hz) was used for the resistance measurements, and a stable base temperature of 1.4 K was obtained by pumping on 4 He liquid. In both pulsed and quasistatic measurements, the current through the sample was driven in the interplane \mathbf{b}^* direction; in such a configuration the measured resistance is accurately proportional to the interplane resistivity component ρ_{zz} [1].

3.2. Pulsed-field magnetotransport: Shubnikov-de Haas and magnetic breakdown oscillations.

Figure 1 shows the magnetoresistance of a λ -(BETS) $_2$ GaCl $_4$ crystal obtained using pulsed magnetic fields; the temperature was 340 mK and the magnetic field was applied parallel to the \mathbf{b}^* direction (*i.e.* perpendicular to the Q2D planes of the crystal) [11]. After the superconducting to normal transition, the resistance rises until a series of low-frequency Shubnikov-de Haas oscillations emerges at about 33 T. These grow in amplitude, until at about 45 T, a higher frequency series of oscillations becomes visible.

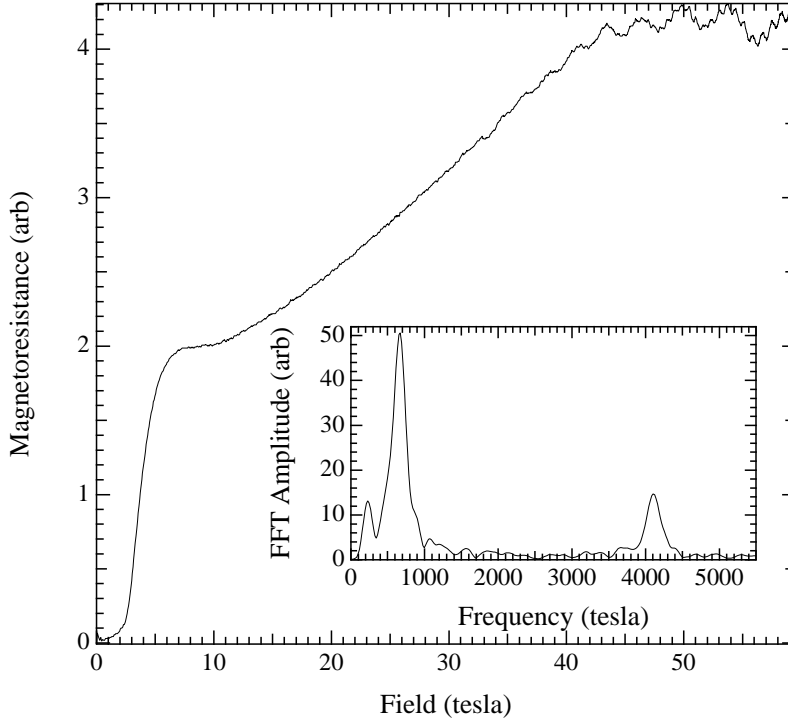


Figure 1. Resistance of an λ -(BETS) $_2$ GaCl $_4$ crystal as a function of magnetic field, applied parallel to the \mathbf{b}^* direction; the temperature is 340 mK. The inset shows a Fourier transform of the data after subtraction of the non-oscillatory background [1]. The peak at 650 T is associated with the α pocket; that at 4030 T is due to the breakdown (β) orbit which encompasses 100 % of the Brillouin zone.

The inset shows a Fourier transform of the magnetoresistance data. The lower of the two frequencies F_α (believed to originate from the α pocket) is 650 ± 5 T. The higher frequency of 4030 ± 25 T, which occurs at fields above ~ 45 T, corresponds to an area in k -space approximately equal to the Brillouin-zone cross-section; following common usage in other charge-transfer salts [1], we will refer to this as the β frequency F_β . Frequencies equivalent to the Brillouin-zone area are readily observed in other charge-transfer salts (typically in κ and α -phase salts of the form (BEDT-TTF) $_2$ X) as a result of magnetic breakdown, whereby electrons tunnel between the Q1D and Q2D sections of the Fermi surface [1].

The observation of magnetic breakdown is not unexpected in this material, given the small size of the gap between the Q2D and Q1D Fermi-surface sections predicted by the bandstructure calculations [12]. However, the experimentally-observed value of $F_\alpha \approx 650$ T is roughly a factor two smaller than that predicted by the calculations. Discrepancies between model and experiment of this size are not unknown in charge-transfer salts [18, 19].

Salt	m_α^*/m_e	F_α (T)	m_β^*/m_e	F_β (T)	T_c (K)	Source
κ -(BEDT-TTF) ₂ Cu(NCS) ₂	3.5	600	6.5	3920	10.4	[21]
λ -(BEDT) ₂ GaCl ₄	3.6	650	6.3	4030	5	present work

Table 1. Comparison of magnetic quantum oscillation frequencies and effective masses in λ -(BEDT)₂GaCl₄ and κ -(BEDT-TTF)₂Cu(NCS)₂. The table shows the effective masses m_α^* and m_β^* and frequencies F_α and F_β corresponding to the α and β orbits of the Fermi surface.

3.3. Effective mass determination.

Although the Fermi surface of λ -(BEDT)₂GaCl₄ is Q2D, the relatively small amplitudes of the oscillations in the magnetoresistance (see Figure 1), and the absence of harmonics in the Fourier transform (inset to Figure 1) imply that the Lifshitz-Kosevich (LK) theory should provide an accurate description of the temperature dependence of the oscillations [1]. According to this theory, the thermal damping factor has the form [20]

$$R_T(B, T) = \frac{\chi(\frac{m^*}{m_e})\frac{T}{B}}{\sinh(\chi(\frac{m^*}{m_e})\frac{T}{B})}, \quad (1)$$

where $\chi = 14.69 \text{ TK}^{-1}$ and m_e is the free electron mass. On fitting the amplitudes of the oscillations as a function of temperature (14 different temperatures ranging from 340 mK to 3.0 K were used) we obtain the effective masses $m_\alpha^* = 3.6 \pm 0.1 m_e$ for F_α and $m_\beta^* = 6.3 \pm 1 m_e$ for F_β .

Table 1 compares the effective masses and Fermi-surface areas obtained in λ -(BEDT)₂GaCl₄ and the most heavily-studied κ -phase BEDT-TTF superconductor, κ -(BEDT-TTF)₂Cu(NCS)₂ [21] (see Section 3.2 of Reference [1] for similar data on other κ -phase BEDT-TTF salts). Note that the Fermi-surface parameters of the two salts are remarkably similar. Moreover, bandstructure calculations in both salts predict $m_\alpha^* \sim m_e$ [12, 21], whereas the observed masses are a factor ~ 3.5 bigger than this, indicating that interactions which renormalise the quasiparticle masses [1, 21, 22] are of similar importance in both materials. In both cases, the bandstructure calculations [12, 21] predict that $m_\beta^* \approx 2m_\alpha^*$, in reasonable agreement with the experimental values, and suggesting that the renormalising interactions influence both Q1D and Q2D Fermi-surface sections in a similar manner [1, 21]. The only marked difference between λ -(BEDT)₂GaCl₄ and κ -(BEDT-TTF)₂Cu(NCS)₂ is the relatively high value of the Dingle Temperature in the former material; the rate of growth of the oscillations with increasing field (see Figure 1) suggests a Dingle temperature of $T_D \approx 3.2 \pm 0.1 \text{ K}$ for the α pocket. Typical values of T_D in κ -(BEDT-TTF)₂Cu(NCS)₂ crystals [1, 23] (and indeed in κ -phase BEDT salts [24]) are often a factor ~ 5 smaller than this, indicating that the impurity scattering rate in λ -(BEDT)₂GaCl₄ is relatively high. The reason for this difference is not yet clear.

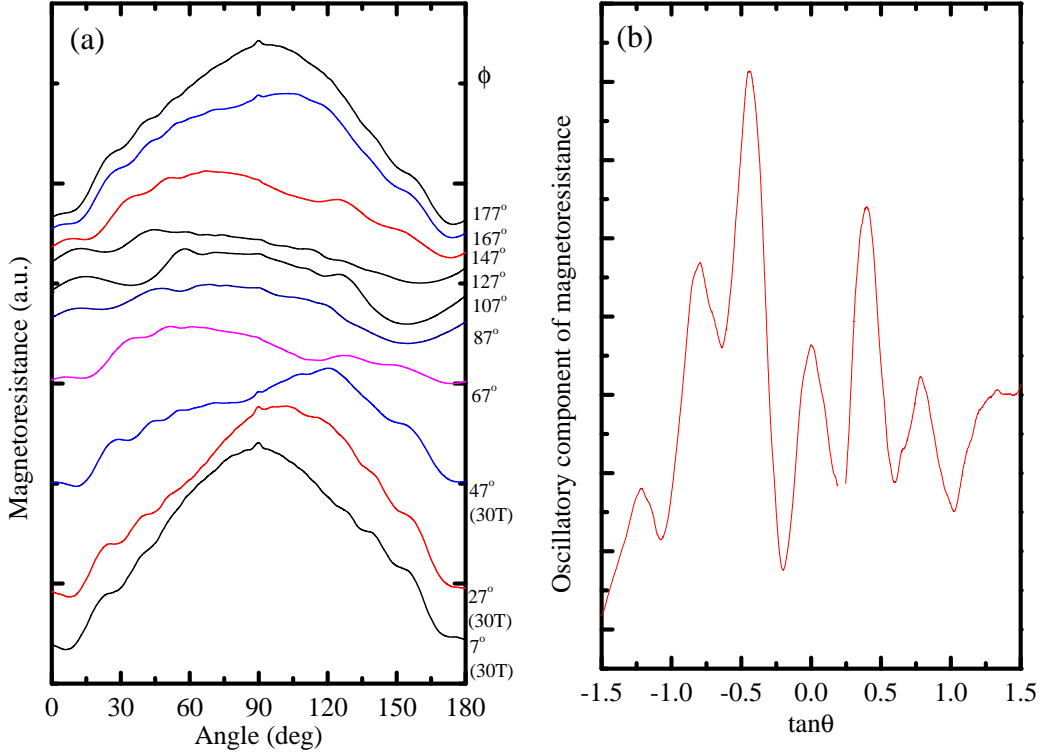


Figure 2. (a) Magnetoresistance of an λ -(BETS) $_2$ GaCl $_4$ crystal as a function of θ , the angle between the applied magnetic field and \mathbf{b}^* . Data are shown for a number of different ϕ angles (listed at right side of the Figure), where ϕ is azimuthal angle between the plane of rotation and the $\mathbf{b}^*\mathbf{c}$ plane. The lowest three traces were recorded at 30 T; the rest of the data were acquired at 27 T. AMROs are observed as gentle oscillations of the resistance, periodic in $\tan\theta$; the small peak at 90° is due to the presence of a small number of closed quasiparticle orbits on the warped Fermi-surface sections. (b) Illustration of the method of locating the AMRO resistance maxima ($\phi = 7^\circ$ data from (a)). The slowly-varying background magnetoresistance has been fitted to a fourth-order polynomial in θ and subtracted from the experimental data, leaving the oscillatory component. Peaks periodic in $\tan\theta$ are plainly visible.

3.4. Angle-dependent magnetoresistance oscillations (AMROs).

Figure 2(a) shows the magnetoresistance of a λ -(BETS) $_2$ GaCl $_4$ crystal as a function of θ , the angle between the applied magnetic field and \mathbf{b}^* . Data are shown for a number of different ϕ angles, where ϕ is azimuthal angle between the plane of rotation and the $\mathbf{b}^*\mathbf{c}$ plane. Distinct AMROs are observed; their ϕ dependence suggests that they are caused by a Q2D Fermi-surface section [1, 19]. In such a case, maxima in the magnetoresistance occur at angles θ_i defined by [1, 19]

$$b'k_{\parallel} \tan \theta_i = \pi(i \pm \frac{1}{4}) + A(\phi), \quad (2)$$

where i is an integer, k_{\parallel} is the maximum Fermi wave-vector projection on the plane of rotation of the field and b' is the effective interplane spacing (see Fig. 2(b)). On plotting the positions of the maxima θ_i versus i , taking account of the correct sign of the $\frac{\pi}{4}$ term [18, 19], we obtain straight lines at all azimuthal angles in accordance with these

expectations. On choosing b' to be interlayer spacing (18.4 Å) obtained from X-ray diffraction studies [12, 15], we obtain the locus for k_{\parallel} versus ϕ shown in Figure 3(a).

A locus in the shape of a figure of eight is the usual result for a pocket of elliptical cross-section [1, 18, 19]. For a pocket of ideal elliptical geometry, the locus of k_{\parallel} is given by

$$k_{\parallel} = [k_x^2 \cos^2(\phi - \xi_{\text{inc}}) + k_y^2 \sin^2(\phi - \xi_{\text{inc}})]^{\frac{1}{2}}, \quad (3)$$

where ξ_{inc} is the inclination of the major axis of the ellipse with respect to $\mathbf{b}^*\mathbf{c}$ plane. The parameters $k_x = 4.86 \pm 0.08 \text{ nm}^{-1}$, $k_y = 1.63 \pm 0.01 \text{ nm}^{-1}$ and $\xi_{\text{inc}} = 19 \pm 5^\circ$ yield the best fit (solid curves in Figure 3(a)).

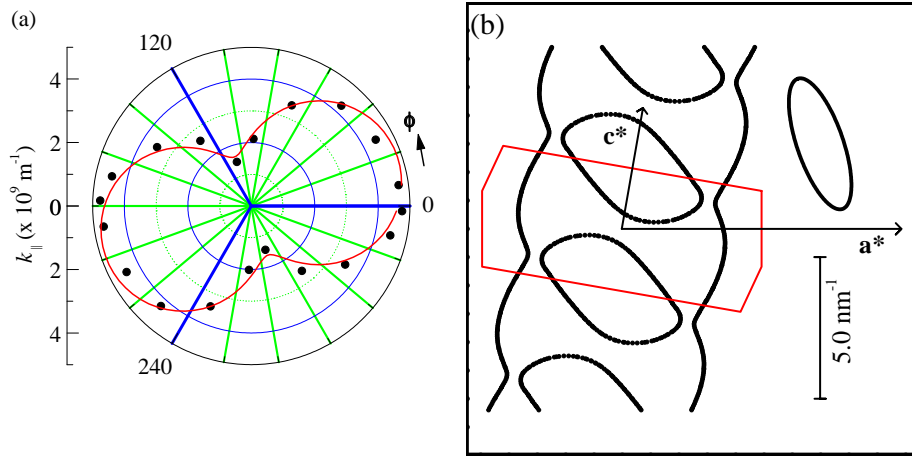


Figure 3. (a) Locus of k_{\parallel} versus azimuthal angle ϕ derived from fits of Equation 2 to the AMRO data. Data are points and the curve is a fit to Equation 3 with the parameters $k_x = 4.86 \pm 0.08 \text{ nm}^{-1}$, $k_y = 1.63 \pm 0.01 \text{ nm}^{-1}$, $\xi_{\text{inc}} = 19 \pm 5^\circ$ and $b' = 18.4 \text{ Å}$. (b) The experimental cross-sectional shape and orientation of the Q2D Fermi-surface pocket, shown alongside (and to the same scale as) the Brillouin zone, reciprocal lattice vectors \mathbf{a}^* , \mathbf{c}^* and calculated Fermi surface of Reference [15]. The pocket is described by the parameters $k_x = 2.43 \pm 0.04 \text{ nm}^{-1}$, $k_y = 0.815 \pm 0.005 \text{ nm}^{-1}$, $\xi_{\text{inc}} = 19 \pm 5^\circ$ and $b' = 2 \times 18.4 \text{ Å} \approx 36.8 \text{ Å}$ (see text and Equation 3).

The values of k_x and k_y deduced from the AMRO data indicate an ellipse area corresponding to a Shubnikov-de Haas frequency of $2608 \pm 60 \text{ T}$. This is almost exactly four times larger than the value of F_α observed in λ -(BETS) $_2$ GaCl $_4$ (see Table 1). It is inconceivable that this value of $\sim 2608 \text{ T}$ could be the actual area of the α pocket, as it would then occupy $\sim 66 \%$ of the Brillouin zone. Quantum oscillation measurements remain the definitive method for obtaining Fermi-surface cross-section areas [1, 20]. On the other hand, the AMRO measurements shown in Figure 2 behave exactly as one would expect for a Q2D Fermi-surface pocket [19], with no evidence for any significant misalignment of the sample; *i.e.* the fits to Equation 2 are straight lines and the peak feature at $\theta \approx 90^\circ$ occurs at 90° for all azimuthal angles.

A possible explanation is that the true interlayer spacing (as perceived by the quasiparticles) is double the unit-cell height, or that there is a modulation of the lattice

in the crystallographic \mathbf{b} direction; this would result in an effective interlayer spacing of $b' = 2 \times 18.4 \text{ \AA} \approx 36.8 \text{ \AA}$. Such a modulation of the lattice could occur in the event of a charge-density-wave (CDW) or spin-density-wave (SDW) instability; however, there is as yet no other evidence for the presence of such a groundstate (*c.f.* numerous other charge-transfer salts in which CDWs or SDWs cause extensive modification of the quantum-oscillation spectrum [1, 25]). If such a modulation exists, it is too weak to be picked up by a careful X-ray study at 115 K (Bruker-AXS SMART6000 CCD, complete sphere of data, sixty-second frames, 0.3 degree scans) [26]. However, this does not rule out the possibility that doubling occurs at a lower temperature [26].

Whatever the mechanism, a doubling of b' (see Equation 2) would result in the Fermi-surface parameters $k_x = 2.43 \pm 0.04 \text{ nm}^{-1}$, $k_y = 0.815 \pm 0.005 \text{ nm}^{-1}$ and $\xi_{\text{inc}} = 19 \pm 5^\circ$, yielding an ellipse area corresponding to a Shubnikov-de Haas frequency of $652 \pm 15 \text{ T}$, in very good agreement with $F_\alpha = 650 \pm 5 \text{ T}$ derived in Section 3.2. Figure 3(b) shows an elliptical-cross-section Q2D pocket of this size and orientation alongside the most recent calculation of the Fermi surface [15], based on structural studies carried out at 17 K. The Q2D pocket measured experimentally is smaller and somewhat more elongated than that suggested by the calculations; it occupies $\approx 16 \%$ of the Brillouin zone, whereas the Q2D pocket of the calculation is 28% of the Brillouin-zone area. However, such discrepancies between calculation and experiment are not without precedent in crystalline organic metals [18, 19, 25].

3.5. Estimate of the interplane transfer integral

We now turn to the small peak in the magnetoresistance component ρ_{zz} observed at $\theta = 90^\circ$ in Figure 2. Thus far, we have treated only the Fermi-surface cross-section in the $\mathbf{a}^*\mathbf{c}^*$ plane (see Figure 3(b)). However, a small, but finite interlayer transfer integral will lead to a warping of the Fermi surface in the interlayer \mathbf{b}^* direction (see Section 2 of Reference [1]). When the magnetic field is almost exactly in the plane of the warping, a few closed orbits become possible on the warped sections of the Fermi surface (e.g. on the “bellies” of the warped Q2D Fermi cylinders) [27, 28, 30]. For certain orientations of an in-plane field, closed orbits will be possible on both the Q1D sheets and Q2D cylinders of a Fermi surface such as that shown in Figure 3(b); at other orientations of an in-plane field, only the Q2D cylinders will be able to support closed orbits on their bellies. Such orbits are very effective at averaging the interplane velocity component v_z , and hence lead to a peak in ρ_{zz} [28, 29, 30].

As the magnetic field is tilted away from the in-plane direction ($\theta = 90^\circ$), the closed orbits will cease to be possible when $\theta = 90^\circ \pm \Delta$, where the angle Δ is given by

$$\Delta(\text{in radians}) \approx \frac{v_\perp}{v_\parallel}, \quad (4)$$

where v_\perp is the maximum interlayer quasiparticle velocity and v_\parallel is the intralayer component of the quasiparticle velocity in the plane of rotation of the magnetic field [28, 29, 30]. If the quasiparticle dispersion $E(k_b)$ in the interlayer direction is

assumed to follow a simple tight-binding model, $E(k_b) = -2t_\perp \cos(k_b b)$ [31], where t_\perp is the interlayer transfer integral, then

$$v_\perp = 2t_\perp b/\hbar, \quad (5)$$

where we have used the relationship $\hbar \mathbf{v} = \nabla_{\mathbf{k}} E(\mathbf{k})$ [31] to obtain v_\perp from $E(k_b)$ [30]. Equations 4 and 5 therefore show that there is a direct proportionality between 2Δ , the angular width of the peak in ρ_{zz} , and the interlayer transfer integral, t_\perp .

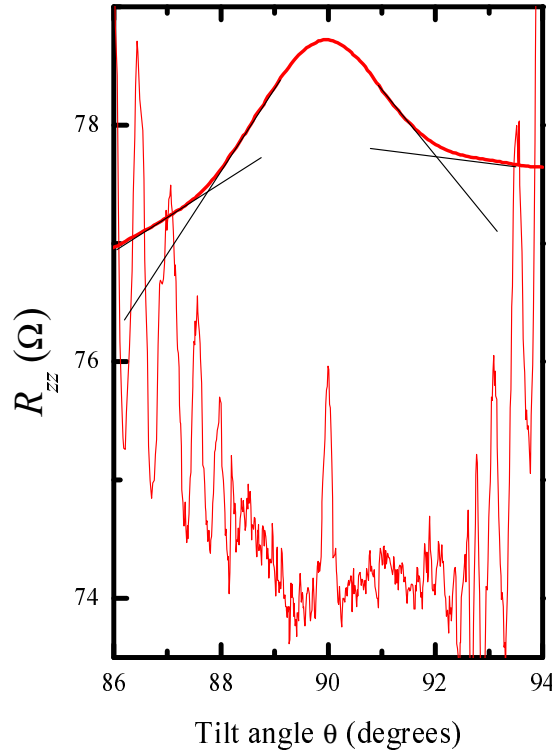


Figure 4. Peaks in the interplane resistance R_{zz} (proportional to ρ_{zz}) close to $\theta = 90^\circ$ in λ -(BETS) $_2$ GaCl $_4$ (thick line; $T = 1.4$ K, $B = 30$ T; present work) and κ -(BEDT-TTF) $_2$ Cu(NCS) $_2$ (fine line; $T = 520$ mK, $B = 42$ T; Reference [30]). In the case of κ -(BEDT-TTF) $_2$ Cu(NCS) $_2$, the rapid oscillations at the edges of the figure are angle-dependent magnetoresistance oscillations (AMROs). The fine lines superimposed on the λ -(BETS) $_2$ GaCl $_4$ data show how the full width of the peak is defined.

Figure 4 shows how the angular width 2Δ of the peak in ρ_{zz} is defined; the limits of the peak are defined by the intersections of extrapolations of the background magnetoresistance and the edges of the peak [32]. Similar data for κ -(BEDT-TTF) $_2$ Cu(NCS) $_2$ from Reference [30] are plotted for comparison; note how the peak at 90° is much narrower. Given the similarity of their intralayer Fermi-surface properties (see Table 1), this comparison immediately suggests a much smaller t_\perp in κ -(BEDT-TTF) $_2$ Cu(NCS) $_2$ than in λ -(BETS) $_2$ GaCl $_4$.

In order to obtain a quantitative estimate of t_\perp , it is necessary to use reliable values of v_\parallel [28, 30]. Figure 3(b) suggests that when the in-plane magnetic field is close to

the \mathbf{a}^* direction, it is likely that *both* Q1D and Q2D Fermi-surface sections will be able to support closed orbits; conversely, when the magnetic field is well away from this orientation, only the Q2D cylinder will be able to support closed orbits. As most of the accurate information deduced from the experiments in the previous Sections concerns the Q2D Fermi-surface section, we concentrate on the range of ϕ over which it alone will determine the peak at $\theta = 90^\circ$.

We assume an effective-mass-tensor approximation for the in-plane motion on the Q2D Fermi-surface section [1];

$$E = \frac{\hbar^2 k_x^2}{2m_1} + \frac{\hbar^2 k_y^2}{2m_2} \quad (6)$$

Here m_1 and m_2 are effective masses *for linear motion* in the x and y directions. The cyclotron effective mass in such an approximation is $m^* = (m_1 m_2)^{1/2}$ [31]. Using the lengths of the axes of the elliptical cross-section of the Q2D Fermi-surface section derived from the AMROs (2.43 nm^{-1} and 0.815 nm^{-1} ; see previous section- we have divided by 2 to account for apparent doubling of the unit-cell height) and $m^* = 3.6 m_e$ (Table 1), we obtain $\frac{m_1}{m_2} = \left(\frac{2.43}{0.815}\right)^2$ and $m_1 m_2 = (3.6 m_e)^2 = 12.96 m_e^2$, yielding $m_1 = 10.73 m_e$, $m_2 = 1.207 m_e$ and $E_F \approx 20.95 \text{ meV}$ (*c.f.* $m_1 = 10.59 m_e$, $m_2 = 1.177 m_e$ and $E_F \approx 18.4 \text{ meV}$ in κ -(BEDT-TTF) $_2$ Cu(NCS) $_2$ [30]). Hence, using $\hbar \mathbf{v} = \nabla_{\mathbf{k}} E(\mathbf{k})$ [31], and constraining $E = E_F$, the velocities $v_{||}(\phi)$ may be derived for the Q2D Fermi-surface section.

The widths 2Δ derived from data such as those in Figure 4 are plotted as a function of ϕ in Figure 5. The Figure also shows the prediction of Equation 4 using $v_{||}$ derived from Equation 6; the only fit parameter is t_{\perp} (see Equation 5). We have chosen to fit data for ranges of ϕ at which the Q2D pocket is expected to be the *sole* provider of closed orbits for in-plane magnetic fields; *i.e.* we avoided field orientations close to $-\mathbf{a}^*$ ($\phi = 90^\circ$) and \mathbf{a}^* ($\phi = 270^\circ$) (dashed lines) at which the Q1D sheets might also be expected to provide closed orbits in an in-plane field (see Figure 3(b)). (Note that the experimental data show a strong peak close to $\phi = 90^\circ$ and 270° (instead of the minimum predicted by the model) suggesting that the Q1D sections are indeed the dominant cause of the peak in ρ_{zz} at these orientations.) The fit yields $v_{\perp} \approx 1200 \text{ ms}^{-1}$, so that $t_{\perp} \approx 0.21 \text{ meV}$ [33]. A similar procedure has been carried out for κ -(BEDT-TTF) $_2$ Cu(NCS) $_2$, giving an interplane transfer integral of $t_{\perp} \approx 0.04 \text{ meV}$ [30]. Therefore, the interplane transfer integral in λ -(BETS) $_2$ GaCl $_4$ is a factor ~ 5 bigger than that in κ -(BEDT-TTF) $_2$ Cu(NCS) $_2$.

3.6. Summary.

In summary, the magnetoresistance measurements indicate that the Fermi surface of λ -(BETS) $_2$ GaCl $_4$ bears a strong resemblance to that of κ -(BEDT-TTF) $_2$ Cu(NCS) $_2$ within the highly-conducting Q2D planes. Moreover, the effective masses in the two salts are almost identical and the renormalising interactions are probably of a similar strength.

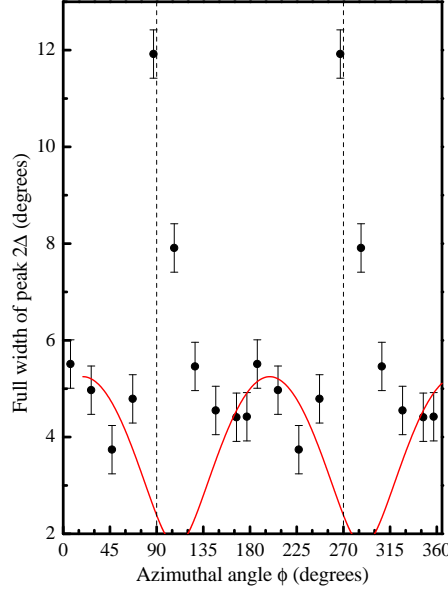


Figure 5. Full widths of peaks in ρ_{zz} close to $\theta = 90^\circ$ for λ -(BETS) $_2$ GaCl $_4$ (points) plotted as a function of ϕ . The curve is given by Equations 4, 5 and 6, with $t_\perp = 0.21$ meV. Note that we have chosen to fit data for ranges of ϕ at which the Q2D pocket is expected to be the *sole* provider of closed orbits for in-plane magnetic fields; *i.e.* we avoided field orientations close to $-\mathbf{a}^*$ ($\phi = 90^\circ$) and \mathbf{a}^* ($\phi = 270^\circ$) (dashed lines) at which the Q1D sheets might also be expected to provide closed orbits in an in-plane field (see Figure 3(b))

The width of the peak in the magnetoresistance close to $\theta = 90^\circ$ suggests that the interplane transfer integral in λ -(BETS) $_2$ GaCl $_4$ is approximately five times bigger than that in κ -(BEDT-TTF) $_2$ Cu(NCS) $_2$. This implies that λ -(BETS) $_2$ GaCl $_4$ is a less two-dimensional material.

4. Penetration-depth measurements.

4.1. Experimental details.

In the current experiments, the penetration depth was inferred by placing the superconducting sample in a small coil which is the inductive element of a resonant tank circuit [34, 35]. The exclusion of flux from the sample, and hence the coil, decreases the inductance of the circuit; consequently the resonant angular frequency, $\omega = 1/\sqrt{LC}$, will increase. The well-known properties of inductors [36] lead to $\frac{\Delta A_\phi}{A_C} = \frac{\Delta L}{L}$, where ΔA_ϕ is the change in flux area, A_C is the area of the measurement coil, ΔL is the change in inductance and L is the total inductance. For small changes in inductance, $\frac{\Delta L}{L_0} = 2\frac{\Delta f}{f_0}$, where Δf is the change in resonant frequency, f_0 is the initial resonant frequency, and L_0 is the initial inductance. Through simple geometrical relations it can be shown that [37]

$$\frac{\Delta A_\phi}{A_C} = \frac{2r_s\Delta\lambda - \Delta\lambda^2}{R^2}, \quad (7)$$

where $\Delta\lambda$ is the change in penetration depth, R is the effective radius of the coil, r_s is the effective sample radius. Simple estimates for the sample sizes used in the current experiments show that the second-order term is negligible [37], so that

$$\Delta\lambda = \frac{R^2}{r_s} \frac{\Delta f}{f_0}. \quad (8)$$

The λ -(BETS) $_2$ GaCl $_4$ samples used in the current study have a needle-like geometry [13]; a typical example had approximate dimensions $2 \times 0.170 \times 0.084$ mm 3 . In order to maximize the filling factor and cross sectional area, the coil was made rectangular, with an effective area of 1.34 mm 2 ; for the sample mentioned above, the effective sample radius is half the shortest dimension (0.042 mm) (note that the long axis of the crystal is perpendicular to the coil axis). Calibration was achieved by placing a spherical superconducting sphere of known size in the coil [2]. The sample was orientated in the coil so that the oscillating magnetic field was parallel to the crystallographic \mathbf{b}^* direction, *i.e.* perpendicular to the highly-conducting planes [11]. The tank-circuit capacitance was provided by a 30 pF mica capacitor, and the circuit was driven at $f \approx 25$ MHz by a tunnel-diode oscillator [34, 38]. The sample and coil were placed in a ^3He cryostat or dilution refrigerator. Quasistatic magnetic fields of up to 30 T were applied parallel to \mathbf{b}^* .

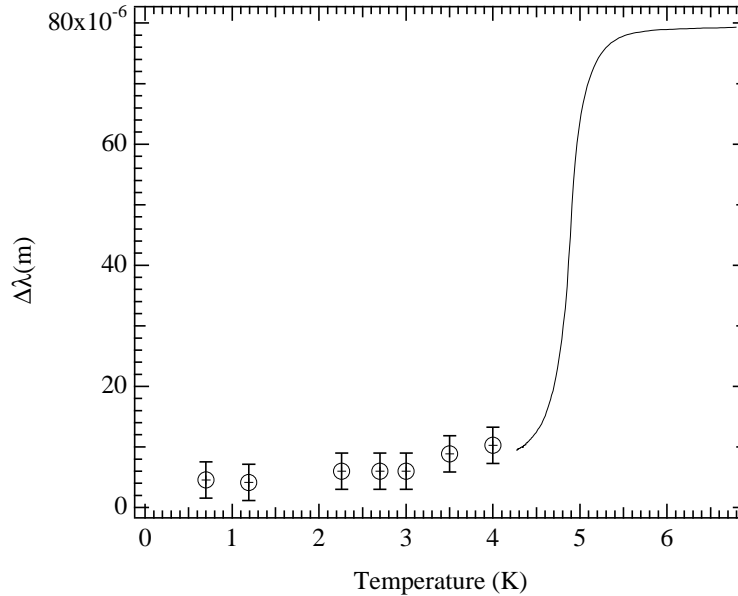


Figure 6. Change in penetration depth versus temperature at zero field in λ -(BETS) $_2$ GaCl $_4$. Note that the cryostat used could only provide controlled, slow sweeps of temperature down to 4.2 K (data shown as continuous curve). Below this, data are recorded at fixed, stable temperatures (points). The error bars on the points give typical uncertainties, valid across the whole temperature range shown.

Figure 6 shows $\Delta\lambda$ of a λ -(BETS) $_2$ GaCl $_4$ crystal (deduced from the frequency of the tank circuit using Equation 8) as a function of temperature. The sharp rise in penetration between 4.5 K and 5.1 K gives a very clear indication of the superconducting

to normal transition; above this temperature $\Delta\lambda \approx 80 \mu\text{m}$ (i.e. comparable to the shortest dimension of the sample), indicating that the radiofrequency fields penetrate the whole crystal once it is in the normal state. This is in agreement with estimates of the low-temperature normal-state conductivity for λ -(BETS) $_2$ GaCl $_4$ [12], which lead one to expect an in-plane skin depth $\delta \sim 100 \mu\text{m}$ [39, 40].

4.2. Measurements at low magnetic fields: determination of pinning parameters

Wu and Sridhar [41] have treated the repulsively interacting flux lines in a type-II superconductor as periodic, damped harmonic-oscillator potentials modulated by a rf field. The physical justification of their model is that the repulsive interaction of the fluxoids causes the Abrikosov lattice [42, 43] to resist higher flux densities in a manner analogous to the way in which a two dimensional network of springs resists compression. In such a model, the Labusch pinning potential parameter α corresponds to the restoring force on fluxoids displaced slightly by the current density J induced by the radiofrequency field [41]: $\eta \frac{dx}{dt} + \alpha x = \phi_0 J$. Here x is the fluxoid displacement, η is a damping parameter and ϕ_0 is the flux quantum [41]. In other words, a small perturbation displaces the fluxoid from its equilibrium position against the restoring force provided by the repulsion from neighbouring fluxoids and the pinning potential.

In the limit of small magnetic field ($H \ll B_{c2}$), the damping due to fluxoid viscous drag [41, 44] may be neglected, leading to a linear relationship between changes in the square of the penetration depth $\Delta\lambda^2$ and the magnetic induction B inside the sample [41],

$$\Delta\lambda^2 = \frac{\phi_0}{\mu_0\alpha(T)} B(H). \quad (9)$$

Figure 7 (inset) shows the field dependence of $\Delta\lambda^2$ at a temperature of $T = 700 \text{ mK}$. The sample is well inside the mixed state for fields above $\mu_0 H \approx 0.01 \text{ T}$, so that $B = \mu_0 H$; hence, the linear dependence predicted by Equation 9 fits the data well, yielding a Labusch parameter of $\alpha(700 \text{ mK}) \approx 1.4 \text{ Nm}^{-2}$.

Data similar to those in the inset of Figure 7 were acquired at a range of temperatures; the resulting values of α are plotted in Figure 7 (main figure) as a function of temperature. The solid line fit through the data in Figure 7 is the predicted temperature dependence from the two-fluid Gorter-Casmir [43, 45] model,

$$\alpha \propto \left[1 - \left(\frac{T}{T_c} \right)^4 \right]. \quad (10)$$

Figure 7 also highlights some of the differences between organic superconductors and the “high- T_c ” cuprates. As $T \rightarrow 0$, the Labusch parameter in λ -(BETS) $_2$ GaCl $_4$ tends to 1.5 Nm^{-2} , almost four orders of magnitude smaller than that in YBa $_2$ Cu $_3$ O $_7$ [41]. Moreover, whereas the two-fluid model is able to describe the λ -(BETS) $_2$ GaCl $_4$ data to a fair degree of accuracy, the pinning-force parameter in YBa $_2$ Cu $_3$ O $_7$ has been shown to follow the temperature dependence $(1 - (T/T_c)^2)^2$ [41].

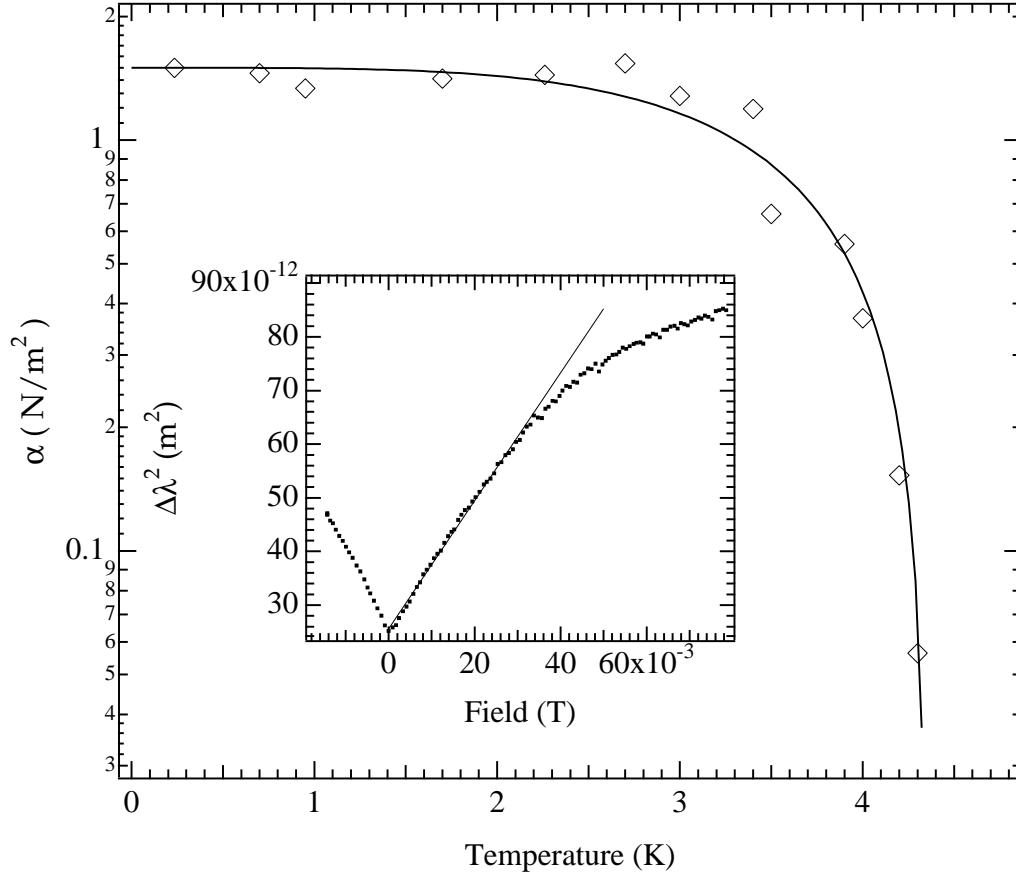


Figure 7. Inset: the determination of the Labush parameter $\alpha(T)$ by a straight line fit to low-field $\Delta\lambda^2$ vs. $\mu_0 H$ data ($T = 700$ mK). Main figure: experimental values of α versus temperature (points); the curve is a fit to the two-fluid model expression.

4.3. Measurements at high magnetic fields: deviation from Campbell penetration-depth behaviour and upper critical field.

Figure 8 shows the measured change in penetration depth $\Delta\lambda$ for λ -(BETS) $_2$ GaCl $_4$ at intermediate fields and a temperature of 700 mK. $\Delta\lambda$ varies approximately as \sqrt{H} , as expected in the Campbell scenario for fluxoid motion [41, 46]. However, above a field which we label $\mu_0 H^*$, $\Delta\lambda$ deviates from the \sqrt{H} dependence; this implies that the periodic harmonic well models [41, 47] are no longer applicable. At fields above $\mu_0 H^*$, $\Delta\lambda$ follows the approximate field dependence H^2 , until the penetration depth saturates.

The identification of the upper critical field in organic superconductors from conductivity data has been the subject of considerable debate [48, 49]; the transition is intrinsically broad, and phenomena such as a pronounced “hump” in the resistivity and negative magnetoresistance are observed close to H_{c2} [1]. (Note that similar complications also afflict the “High- T_c ” cuprates [50, 51].) Recently, a consensus has emerged whereby most of the transition region between zero resistance and normal-state magnetoresistance is regarded as a property of the mixed phase (see References [35, 49]

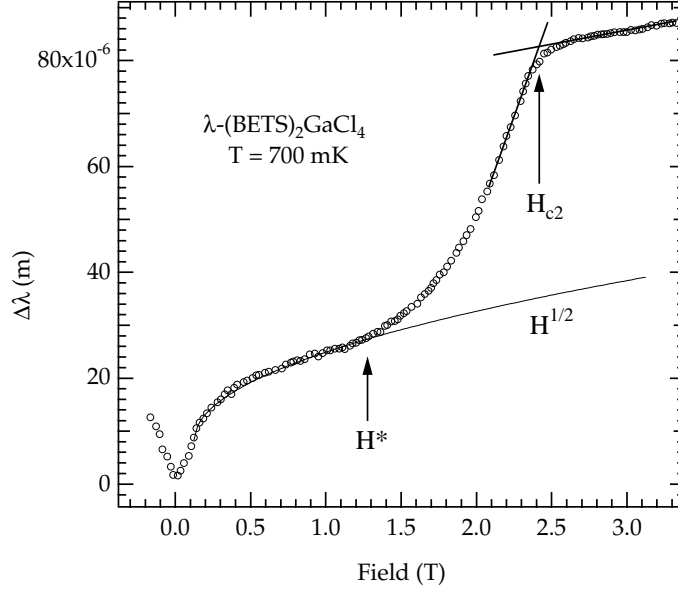


Figure 8. The change in penetration depth signal vs. field for λ -(BETS) $_2$ GaCl $_4$ at 700 mK. The deviation from the Campbell penetration depth behavior is indicated as H^* while the saturation of $\Delta\lambda$ signal indicates H_{c2} , determined from the straight line intercepts.

and references therein); H_{c2} is then defined as the intersection of the extrapolations of the transition region and the normal-state magnetoresistance [35].

In penetration depth measurements, the broadening is less severe since the measurement is not dependent on a macroscopic net current flow across the sample [41, 49]. The pinned fluxoids probed by rf fields do not experience as large an electric field gradient and hence the dissipation associated with the normal core is reduced [41, 49]. Nevertheless, the transition is still somewhat broadened, and so we follow the same spirit of the convention used in resistivity studies [35] and the GHz penetration depth studies of Reference [49], defining H_{c2} as the intersection of extrapolations of the penetration-depth curves below and above the point at which the saturation occurs (see Figure 8). We can be confident that the saturated behaviour is characteristic of the normal state, as it continues up to at least 30 T without further features. This strongly suggests that the whole of the sample is penetrated by the rf fields in the normal state, as suggested in Section 4.1.

The values of H_{c2} and H^* deduced from the penetration depth measurements are shown as a function of temperature in Figure 9. Four different λ -(BETS) $_2$ GaCl $_4$ samples, taken from four separate growth batches, were used in the study. There were negligible differences in their behaviour, and the data from the four samples in Figure 9 overlaid each other, suggesting that the characteristic fields measured are intrinsic properties of λ -(BETS) $_2$ GaCl $_4$. We shall return to the temperature dependence of H_{c2} in a later section.

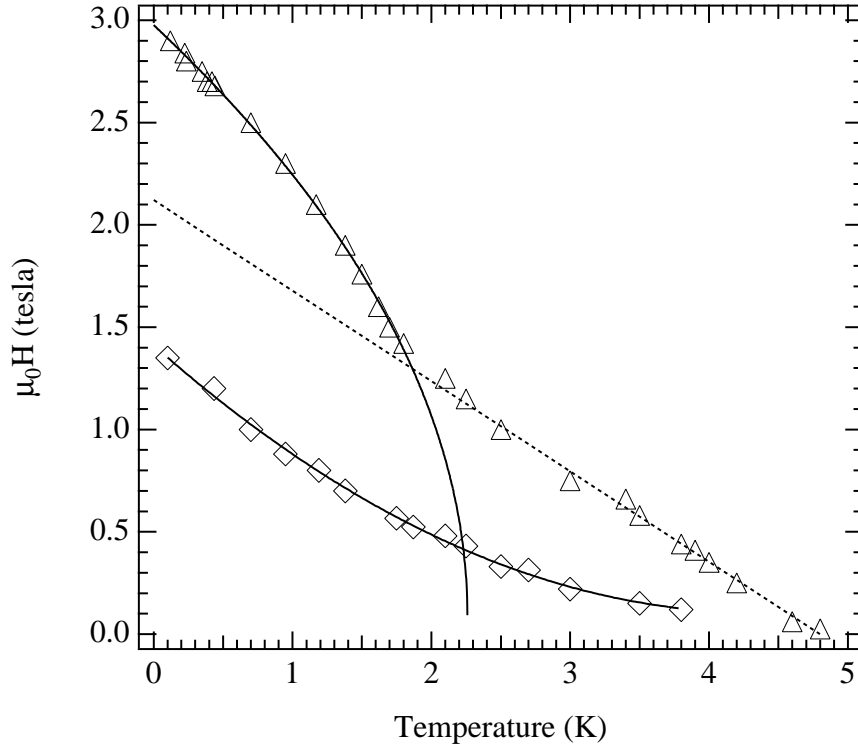


Figure 9. Notional phase diagram of λ -(BETS) $_2$ GaCl $_4$ showing the upper critical field (triangles) and H^* , marking the inflection points in the penetration depth (diamonds). The quasistatic field is applied parallel to \mathbf{b}^* , *i.e.* perpendicular to the quasi-two-dimensional planes of the sample. Points from four different samples are shown, often overlaying each other. The upper solid curve is $H_{c2} \propto (T^* - T)^{1/2}$; the dashed curve is $H_{c2} \propto (T_{c2} - T)$. The lower solid curve is a fit of the two-fluid model expression for the flux-line lattice melting.

4.4. Flux-lattice melting at H^* .

We now turn to the change in behaviour which occurs at the field H^* (see Figure 8). We attribute the change at H^* to flux-line lattice melting, as H^* follows the $(T_c - T)^2$ dependence expected from the Gorter-Casimir two-fluid model [45].

Additional support for this attribution comes from considering microscopic models of the melting process. Houghton *et al.* [52] have considered the elastic moduli of the flux-line lattice and proposed that melting occurs when the mean thermal flux-line displacement $d(T)$ is a substantial fraction of the Abrikosov lattice parameter $\ell = (2\phi_0/\sqrt{3}B)^{1/2}$, *i.e.*, $d(T) \approx c_L \ell$. Here c_L is the Lindemann parameter [53], a function used very generally in the description of solid-liquid transitions; typically $c_L \sim 0.1 - 0.2$. The explicit expression for $d(T)$ is

$$d(T) = \sqrt{\frac{1}{2\pi} \left(\frac{G_i}{\gamma^2} \right)^{1/2} \frac{t}{(1-t)^{1/2}} \frac{b}{(1-b)} \left(\frac{4(\sqrt{2}-1)}{(1-b)^{1/2}} + 1 \right) \ell^2} \quad (11)$$

where $t = T/T_c$ and $b = B/B_{c2}$. The parameter $G_i = (16\pi^3\kappa^4(k_B T)^2)/(\phi_0^3 H_{c2}(0))$ describes the importance of fluctuations in a given system; γ is the anisotropy term

defined by

$$\gamma \equiv \frac{\xi_{xy}}{\xi_z}, \quad (12)$$

with ξ_{xy} and ξ_z being the in-plane and interplane coherence lengths respectively. κ is another Ginzburg-Landau parameter giving the ratio of penetration depth to the coherence length for a particular orientation [43, 52]. In this case we require $\kappa = \frac{\lambda}{\xi_\perp}$. Using Ginzburg-Landau theory in the limit $T \rightarrow 0$ [66] yields $\xi_\perp \approx 1.4$ nm and $\lambda \approx 150$ nm for λ -(BETS) $_2$ GaCl $_4$, resulting in $\kappa \approx 107$.

In this model, the melting field at each temperature can be interpreted as the point at which the product of c_L and the lattice spacing is roughly equal to the average flux line displacement. Thus, an increasing field reduces the average inter-vortex spacing, thereby facilitating melting [52]. Substituting $\mu_0 H^* \approx 1$ T at $T = 700$ mK and $\kappa = 107$ into the above equations yields a flux-line displacement of approximately 6.0 nm, roughly 12% of the Abrikosov lattice spacing. This implies that $c_L \approx 0.12$, a value entirely typical of a solid-liquid transition [53].

In isotropic superconducting systems, the melting of the flux-line lattice occurs so close to H_{c2} as to be indistinguishable from it [43]. However, in materials such as λ -(BETS) $_2$ GaCl $_4$ (and in κ -(BEDT-TTF) $_2$ Cu(NCS) $_2$; see References [56, 59]), the large anisotropy of the superconducting properties permits the melting line to be observed over extended regions of the $H - T$ phase diagram, well clear of H_{c2} .

5. Discussion: comparison of λ -(BETS) $_2$ GaCl $_4$ with κ -(BEDT-TTF) $_2$ Cu(NCS) $_2$; dimensional cross-over.

Having seen in Section 3 that the Fermi surfaces of λ -(BETS) $_2$ GaCl $_4$ and κ -(BEDT-TTF) $_2$ Cu(NCS) $_2$ bear some striking similarities within the Q2D planes but have interplane transfer integrals differing by a factor ~ 5 , it is interesting to compare their superconducting properties.

The work of Belin *et al.* [49] has shown that conventional resistivity measurements can yield unrepresentative values for the upper critical field of κ -(BEDT-TTF) $_2$ Cu(NCS) $_2$ (see also [51, 61]); the difficulties result from the dissipative mechanisms mentioned in Section 4.3, which act to broaden the resistive transition [1, 48]. Thermal conductivity, magnetisation and penetration depth measurements seem to be less susceptible to these problems and give a better reflection of the true H_{c2} [49]. We have therefore compiled the $H_{c2}(T)$ plot in Figure 10 using available thermal conductivity [49], magnetisation [56, 57] and MHz [55] and microwave (12–25 GHz) [49] penetration measurements. There is some scatter amongst the data from different measurements, but all suggest that $(\partial H_{c2}/\partial T)$ increases in magnitude as T increases, and in fact the power law $H_{c2} \propto (T_c - T)^{2/3}$ is quite successful in describing the data (Figure 10).

A material made up of weakly-coupled superconducting planes may transform from a three-dimensional system to what is in effect a series of two-dimensional

superconductors as the interlayer coherence length decreases with decreasing temperature [63]. The dimensional crossover occurs when the interplane coherence length ξ_z becomes shorter than the interplane spacing of the quasi-two-dimensional layers. Muon-spin rotation studies [58] have shown that this transition occurs in κ -(BEDT-TTF) $_2$ Cu(NCS) $_2$ at magnetic fields ~ 7 mT, *i.e.* three orders of magnitude smaller than typical values of H_{c2} (Figure 10). This strongly suggests that the variation of H_{c2} shown in Figure 10 is typical of a quasi-two-dimensional superconductor consisting of weakly-coupled layers [56, 59, 62].

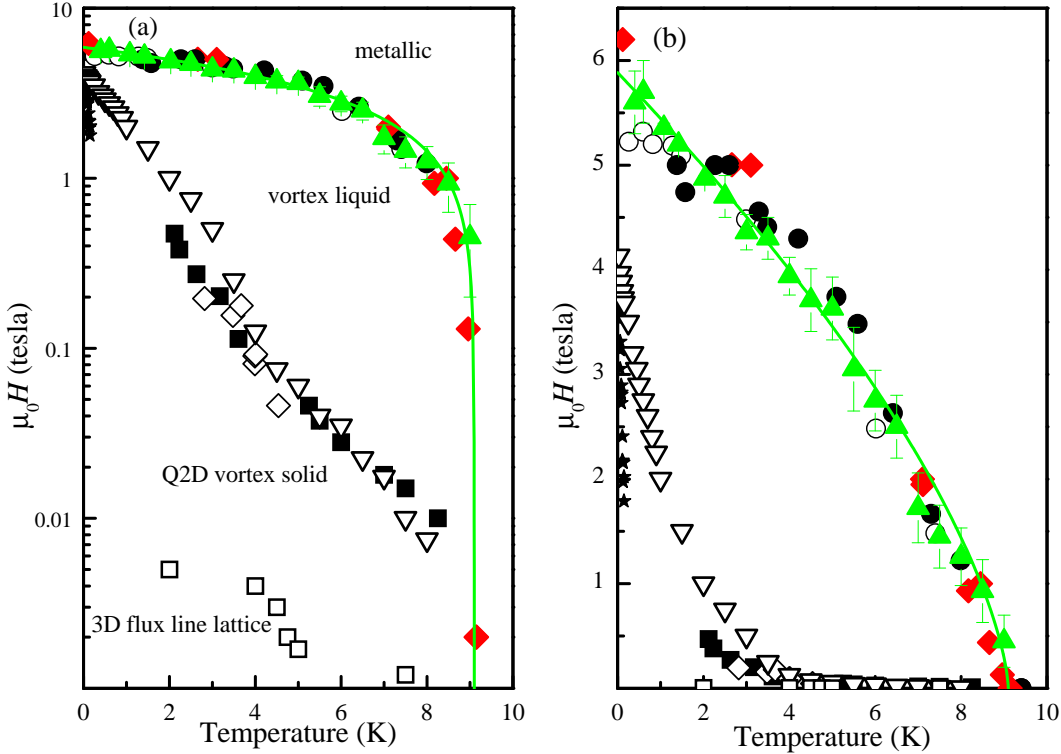


Figure 10. Critical fields in κ -(BEDT-TTF) $_2$ Cu(NCS) $_2$, plotted on logarithmic (a) and linear (b) field scales. The data for H_{c2} comprise filled triangles (MHz penetration data obtained using the apparatus described in the current paper [55]) filled circles (microwave penetration studies; Reference [49]; errors in $\mu_0 H_{c2}$ values typically ± 0.5 T), open circles (thermal conductivity data of Reference [49]; errors not given) and shaded diamonds (magnetisation data; the lowest temperature point was determined by examining the attenuation of de Haas-van Alphen oscillations [56] and the higher-temperature points are from the scaling studies in Reference [57]). The solid curve is proportional to $(T_c - T)^{2/3}$, with $T_c = 9.1$ K. The triangles are the irreversibility field from magnetisation [56]; the filled squares and stars represent 2D melting from magnetometry and GHz studies [59] (see also the NMR data of Reference [60]). The hollow squares are from muon-spin rotation [58] and denote the 3D-2D transition.

Figure 9 shows that the upper critical field of λ -(BETS) $_2$ GaCl $_4$ (conducting planes perpendicular to the applied magnetic field) has a linear region $H_{c2} \propto (T_c - T)$ that spans from T_c to approximately 1.9 K. Below 1.9 K, a definite change in the slope of the upper critical field occurs, and H_{c2} begins to follow the power law $H_{c2} \propto (T^* - T)^\zeta$,

with T^* a fit parameter; powers ζ in the range 0.5 – 0.7 provide an adequate fit to the data.

The behaviour of H_{c2} in λ -(BETS) $_2$ GaCl $_4$ at temperatures below 1.9 K is therefore very similar to that of H_{c2} in κ -(BEDT-TTF) $_2$ Cu(NCS) $_2$ over the whole temperature range shown in Figure 10, and is thus characteristic of a two-dimensional superconductor with weakly-coupled layers [59, 62]. On the other hand, the linear variation of H_{c2} in λ -(BETS) $_2$ GaCl $_4$ at higher temperatures follows the expectations of Ginzberg-Landau theory for three-dimensional superconductors [43, 67]. We therefore attribute the change in gradient at 1.9 K to dimensional cross-over from quasi-two-dimensional (low temperatures) to three dimensional (high temperatures). As we shall now show, this is entirely consistent with estimates of the interplane coherence length in λ -(BETS) $_2$ GaCl $_4$.

The magnetic-field-orientation dependence of B_{c2} [37] in λ -(BETS) $_2$ GaCl $_4$ is qualitatively similar to the predictions of the Ginzberg-Landau anisotropic effective mass approximation [43, 64, 65, 68]

$$B_{c2}(\theta) = \frac{B_{c2}(\theta = 0)}{\sqrt{\cos^2(\theta) + \gamma^{-2} \sin^2(\theta)}}, \quad (13)$$

where θ is the angle between \mathbf{b}^* and the applied magnetic field and γ has been defined in Equation 12. Using Ginzberg-Landau theory [43], the in-plane coherence length may be estimated from the upper critical field when the magnetic field is parallel to \mathbf{b}^* :

$$H_{c2}(\theta = 0) = \frac{\phi_0}{2\pi\xi_{xy}^2}. \quad (14)$$

Fits of the θ dependence of H_{c2} at $T = 1.75$ K [54, 68] (the temperature at which the change in gradient in Figure 9 occurs) yield $\xi_z \approx 1.85$ nm, almost identical with the interplane spacing, and supporting our assertion that the change in gradient in Figure 9 at 1.9 K is associated with a dimensional crossover.

Dimensional crossovers with the magnetic field applied perpendicular to the Q2D planes have been observed in artificial Q2D superconducting structures [69, 70] and in organic superconductors such as κ -(BEDT-TTF) $_2$ Cu(NCS) $_2$ [58, 59]; however, in the majority of these cases, the effect of the crossover is observed at magnetic fields less than H_{c2} . λ -(BETS) $_2$ GaCl $_4$ is perhaps unique in providing the correct anisotropy for the crossover to be observed in the behaviour of $H_{c2}(T)$.

In Section 3.5 we demonstrated that the interplane transfer integral in λ -(BETS) $_2$ GaCl $_4$ is a factor ~ 5 larger than that in κ -(BEDT-TTF) $_2$ Cu(NCS) $_2$. The greater “three dimensionality” of the bandstructure of λ -(BETS) $_2$ GaCl $_4$ compared to κ -(BEDT-TTF) $_2$ Cu(NCS) $_2$ obviously manifests itself in the superconducting behaviour (compare Figures 9 and 10); whereas λ -(BETS) $_2$ GaCl $_4$ exhibits 2D-3D dimensional crossover in its $H_{c2}(T)$ behaviour, $H_{c2}(T)$ in κ -(BEDT-TTF) $_2$ Cu(NCS) $_2$ is entirely characteristic of a Q2D superconductor.

6. Summary

In summary, we have measured the Fermi surface topology of the organic superconductor λ -(BETS) $_2$ GaCl $_4$ using Shubnikov-de Haas and angle-dependent magnetoresistance oscillations. The data show that the Fermi-surface topology of λ -(BETS) $_2$ GaCl $_4$ is very similar indeed to that of the most heavily-studied organic superconductor, κ -(BEDT-TTF) $_2$ Cu(NCS) $_2$, except in one important respect; the interplane transfer integral in λ -(BETS) $_2$ GaCl $_4$ is a factor ~ 5 larger than that in κ -(BEDT-TTF) $_2$ Cu(NCS) $_2$. The increased three-dimensionality of λ -(BETS) $_2$ GaCl $_4$ is manifested in radiofrequency penetration-depth measurements, which show a clear dimensional crossover in the behaviour of H_{c2} . The radiofrequency measurements have also been used to extract the Labusch parameter determining the fluxoid interactions as a function of temperature, and to map the flux-lattice melting curve.

We have observed a discrepancy between the angle-dependent magnetoresistance oscillation and Shubnikov-de Haas data which suggests that the true unit cell height at low temperatures is double that inferred from X-ray studies. At present, this has not been detected by other techniques.

It is interesting to note that the anisotropies and Ginzberg-Landau parameters of the organic superconductors λ -(BETS) $_2$ GaCl $_4$ (this work) and κ -(BEDT-TTF) $_2$ Cu(NCS) $_2$ [58, 56, 59] span the typical values found in “High T_c ” cuprates such as YBCO and BISCCO [43]. However, as the current work has shown, in contrast to the cuprates, the Fermi-surface topologies and complete phase diagrams of organic superconductors such as λ -(BETS) $_2$ GaCl $_4$ and κ -(BEDT-TTF) $_2$ Cu(NCS) $_2$ can be mapped out in detail using accessible laboratory fields. Moreover, details of the bandstructure in the organics can be related directly to the superconducting properties. The availability of a large number of organic superconductors of varying dimensionality and bandstructure [1, 23] should potentially allow very stringent experimental tests of models of superconductivity in layered materials to be carried out.

7. Acknowledgements.

This work is supported by the Department of Energy, the National Science Foundation (NSF), the State of Florida and EPSRC (UK). Acknowledgement is made to the donors of The Petroleum Research Fund, administered by the ACS, for partial support of this research. CHM thanks J.S. Brooks for very useful insights into the radiofrequency measurement technique. We are grateful to Stephen Hill and Monty Mola for their considerable help in compiling Figure 10 and Kazumi Maki, Ross McKenzie and Stephen Blundell for illuminating discussions. Paul Goddard, Mike Whangbo and J.-H. Koo are thanked for permission to use data and calculations from References [15, 30] prior to publication. Finally, we acknowledge the suggestions of one of the Referees, which have helped to clarify several points.

8. Appendix: a note on the radiofrequency response.

In the current paper we have extracted parameters which describe the superconducting state of λ -(BETS) $_2$ GaCl $_4$ under the assumption that all of the apparent changes in the penetration of the radiofrequency field are due to the variation of λ . It is therefore very important to assess whether this assumption is valid. Moreover, as little has been written in the literature about the radiofrequency techniques employed, it is useful to summarise the artefacts which can affect the experimental data. For future reference, we hope that it is also useful to provide estimates of some of the parameters used in the theory used to model experimental data [47].

Coffey and Clem [47] have treated the behaviour of a superconductor in a rf field over a broad frequency range. Using their approach, the contributions to the penetration depth signal from surface-impedance and skin-depth effects can be evaluated as the temperature or applied magnetic field are varied. The model defines boundaries at which the surface-impedance and skin-depth effects become non-negligible; these are set by evaluating the flux creep factor [47].

The flux creep factor ε is determined by ν , the ratio of the fluxoid barrier height U_0 to the typical thermal energy $k_B T$, $\nu = \frac{U_0}{2k_B T}$. The flux creep factor is then determined by: $\varepsilon = 1/I_0(\nu)^2$, where I_0 is a zeroth-order modified Bessel function of the first kind [47]. ε parameterises the degree to which thermal effects assist the motion of fluxoids.

In the limit of large ε (*i.e.* $\varepsilon \sim 1$), thermal excitation causes the behaviour of fluxoids to approach that of completely unpinned fluxoids. In this case, the complex effective resistivity ($\tilde{\rho}_v(\omega)$) becomes a contributing factor to the measured change in penetration depth. $\tilde{\rho}_v(\omega)$ [47] is given by the expression

$$\tilde{\rho}_v(\omega) = \frac{\varepsilon + (\omega\tau)^2 + i(1 - \varepsilon)\omega\tau}{1 + (\omega\tau)^2} \rho_f, \quad (15)$$

where $\rho_f = B\phi_0/\eta$ is the flux flow resistivity and $\omega\tau$ represents the product of the measurement frequency and the relaxation time of the normal-state quasiparticles.

An order-of-magnitude estimate of U_0 is given by considering the energy at which the harmonic-oscillator potentials of neighbouring fluxoids cross, yielding [41] $U_0 \approx \frac{2}{\pi^2} \alpha L^3$. The characteristic length L [41] will be roughly equal to the Abrikosov lattice spacing, $L = \ell$, so that the pinning well barrier height U_0 can be estimated using

$$U_0 = \frac{2\alpha}{\pi^2} \left(\frac{2}{\sqrt{3}} \frac{\phi_0}{B} \right)^{3/2}. \quad (16)$$

Equation 16 shows that U_0 decreases as the field B increases, so that the surface-impedance and skin-depth effects will be most prominent at high magnetic fields. Within the superconducting state, the highest field (*i.e.* worst-case scenario) at which we make quantitative deductions about vortex behaviour is $\mu_0 H^*$, the field at which the penetration depth indicates a divergence from the Campbell regime. Substituting the value for 700 mK, we obtain $U_0 \sim 16$ K. At this field and temperature, $\nu \sim 4$, leading to $\varepsilon \sim 0.005$.

Equation 15 also shows that the value of $\omega\tau$ contributes to the complex resistivity. Taking a frequency $\omega/2\pi \approx 25$ MHz from the current experiments and τ from measurements of the normal-state resistivity [12] (or the penetration depth: see Figure 6), we obtain $\omega\tau \sim 0.005$. Therefore, the fact that both ε and $\omega\tau$ are $\ll 1$ indicates that the surface-impedance and skin-depth effects have negligible impact [47] on the experiments on λ -(BETS) $_2$ GaCl $_4$ reported in this work.

9. References

- [1] J. Singleton, Reports on Progress in Physics **63**, 1111 (2000).
- [2] A. Carrington, I.J. Bonalde, R. Prozorov, R.W. Gianetta, A.M. Kini, J. Schlueter, H.H. Wang, U. Geiser and J.M. Williams, Phys. Rev. Lett., **83**, 4172 (1999).
- [3] H. Elsinger, J. Wosnitza, S. Wanka, J. Hagel, D. Schweitzer and W. Strunz, Phys. Rev. Lett. **84**, 6098 (2000).
- [4] K. Ichimura *et al.*, *Synth. Met.* **103**, 1812 (1999); *Journal-of-Superconductivity*, **12**, 519 (1999); T. Arai *et al.*, Phys. Rev. B **63**, 104518 (2001).
- [5] S. Lefebvre, P. Wzietek, S. Brown, C. Bourbonnais, D. Jerome, C. Meziere, M. Fourmigue and P. Batail, Phys. Rev. Lett. **85**, 5420 (2000).
- [6] Jörg Schmalian, Phys. Rev. Lett. **81**, 4232 (1998).
- [7] Kazuhiko Kuroki and Hideo Aoki, Phys. Rev. B **60**, 3060 (1999).
- [8] K. Maki, E. Puchkaryov, H. Won, *Synth. Met.* **103**, 1933 (1999).
- [9] R. Louati, S. Charfi-Kaddour, A. Ben Ali, R. Bennaceau and M. Heritier, Synthetic Metals **103**, 1857 (1999).
- [10] R. Kato, H. Kobayashi and A. Kobayashi, Synth. Met. **42**, 2093 (1991).
- [11] L. K. Montgomery, T. Burgin, J. C. Huffman, K. D. Carlson, J. D. Dudek, G. A. Yanconi, L. A. Menga, P. R. Mobley, W. K. Kwok, J. M. Williams, J. E. Schirber, D. L. Overmyer, J. Ren, C. Rovira, and M. -H. Wangbo, Synth. Met. **56** 2090 (1993).
- [12] L. K. Montgomery, T. Burgin and J. C. Huffman, J. Ren and M. -H. Whangbo, Physica C **219**, 490 (1994).
- [13] H. Kobayashi, T. Udagawa, H. Tomita, K. Bun, T. Naito and A. Kobayashi, Chem. Lett. **1993**, 1559 (1993)
- [14] Uji *et al.* have recently observed what is believed to be magnetic field-induced superconductivity in λ -(BETS) $_2$ FeCl $_4$ (see S. Uji *et al.*, Nature, **410**, 908 (2001)). However, this salt is not a superconductor at zero field.
- [15] M.-H. Whangbo, H.-J. Koo and L.K. Montgomery, to be published (2001).
- [16] L.K. Montgomery, , T. Burgin, T. Miebach, D. Dunham and J.C. Huffman, Mol. Cryst. Liq. Cryst. **284**, 73(1996).
- [17] F. Herlach, Reports on Progress in Physics, **62**, 859 (1999).
- [18] A. A. House, N. Harrison, S. J. Blundell, I. Deckers, J. Singleton, F. Herlach, W. Hayes, J. A. A. J. Perenboom, M. Kurmoo and P. Day, *Phys. Rev. B* **53**, 9127 (1996).
- [19] M.S. Nam, S.J. Blundell. A. Ardavan, J.A. Symington and J. Singleton, J. Phys: Condens. Matter **13**, 2271 (2001)
- [20] *Magnetic oscillations in metals* D. Shoenberg, (Cambridge University Press, 1984).
- [21] J.M. Caulfield, W. Lubczynski, F.L. Pratt, J. Singleton, D.Y.K. Ko, W. Hayes, M. Kurmoo and P. Day, J. Phys.: Condens. Matter **6**, 2911 (1994).
- [22] K.F. Quader, K.S. Bedell, G.E. Brown, Phys. Rev. B **36**, 156 (1987); A.J. Leggett, Annals of Physics **46**, 76 (1968); W. Kohn, Phys. Rev. **123**, 1242 (1961); K. Kanki and K. Yamada, J. Phys. Soc. Jpn. **66**, 1103 (1997).
- [23] *Fermi surfaces of low-dimensional organic metals and superconductors*, J. Wosnitza (Springer-Verlag, Berlin, 1996)

- [24] C. H. Mielke, N. Harrison, D. G. Rickel, A. H. Lacerda, R. M. Vestal, and L. K. Montgomery, Phys. Rev. B **56**, R4309 (1997).
- [25] N. Harrison, E. Rzepniewski, J. Singleton, P.J. Gee, M.M. Honold, P. Day and M. Kurmoo, J. Phys.: Condens. Matter, **11**, 7227 (1999).
- [26] Unpublished results of L.K. Montgomery and J.C. Huffman (2001).
- [27] For a discussion of the issue of interplane dispersion in quasi-two-dimensional metals and measurements such as this one, see P. Moses and R.H. McKenzie, Phys. Rev. B **60**, 7998 (1999); D. Yoshioka, J.Phys. Soc. Jpn **64**, 3168 (1995); R.H. McKenzie and P. Moses, Phys. Rev. Lett.**81**, 4492 (1998); Phys. Rev. B **60**, 11241 (1999).
- [28] T. Osada *et al.*, Phys. Rev. Lett. **77**, 5261 (1996); N. Hanasaki *et al.*, Phys. Rev. B **57**, 1336 (1998); *ibid.* **60**, 11210 (1999)
- [29] Others propose that “self-crossing orbits” are more effective than closed orbits in averaging v_{\perp} ; however, the geometrical constraints on the peak in ρ_{zz} are identical. See V.G. Peschansky and M.V. Kartsovnik, Phys. Rev. B **60**, 11207 (1999); I.J. Lee and M.J. Naughton, Phys. Rev. B **57**, 7423 (1998).
- [30] J. Singleton, P.A. Goddard, A. Ardavan, N. Harrison, S.J. Blundell, J.A. Schlueter and A.M. Kini, cond-mat/0104570 (2001), Phys. Rev. Lett., submitted; P. Goddard, A. Ardavan, J. Singleton and J.A. Schlueter, to be published.
- [31] *Solid State Physics*, by N.W. Ashcroft and N.D. Mermin (Holt-Saunders, New York, 1976).
- [32] Alternative methods, such as the fitting of more complex functions to the background magnetoresistance and peak yielded negligible gains in accuracy and reproducibility, and were more time-consuming.
- [33] The value $t_{\perp} = 0.21$ meV assumes that the interplane distance b which dominates the interlayer transport is that given by X-ray crystallography, 18.4 Å.
- [34] C.T. VanDeGrift, Rev. Sci. Inst., **46**, 599 (1975); C.T. VanDeGrift, and D.P. Love, Rev. Sci. Inst. **52**, 712 (1981).
- [35] J. Singleton, J.A. Symington, M.S. Nam, A. Ardavan, M. Kurmoo and P. Day, J. Phys.: Condens Matter **12** L641 (2000).
- [36] See *e.g. Electricity and Magnetism*, B.I. Bleaney and B. Bleaney, Oxford University Press (third edition, Oxford, 1990).
- [37] C.H. Mielke, PhD Thesis, Clark University 1996.
- [38] It should be emphasised that this measurement technique represents a very weak perturbation of the sample. The radio-frequency (rf) magnetic field in the coil is ~ 1 μ T, several orders of magnitude smaller than typical applied fields. Moreover, the data were taken at a frequency of 25 MHz, whilst a BCS estimate of the pair-breaking frequency in λ -(BETS)₂GaCl₄ is ~ 160 GHz [37], *i.e.* the measurement frequency is insufficient to cause pair-breaking.
- [39] J.M. Schrama, J. Singleton, R.S. Edwards, A. Ardavan, E. Rzepniewski, R. Harris, P. Goy, M. Gross, J. Schlueter, M. Kurmoo and P. Day, J. Phys.: Condens. **13** 2235 (2001)
- [40] S. Hill, Phys. Rev. B **62**,8699 (2000).
- [41] D. Wu and S. Sridhar, Phys. Rev. Lett., **65** 2074 (1990).
- [42] A. A. Abrikosov, Zh. Eksperim. i Teor. Fiz. **32** 1442 (1957).
- [43] M. Tinkham, *Introduction to superconductivity*, 2nd ed., (McGraw Hill, 1996).
- [44] J. Bardeen and M. J. Stephen, Phys. Rev. **140** A1197 (1965).
- [45] C. J. Gorter and H. B. G. Casimir, Phys. Z. **35** 963 (1934).
- [46] A.M. Campbell and J.E. Evetts, Adv. Phys. **21**, 199 (1972).
- [47] M. W. Coffey and J. R. Clem, Phys. Rev. Lett., **67** 386 (1991).
- [48] H. Ito, T. Ishiguro, T. Komatsu, G. Saito and H. Anzai, Physica B **201**, 470 (1994) and references therein; T. Ishiguro, H. Ito, Yu.V. Sushko, A. Otsuka and G. Saito, Physica B **197**, 563 (1994); F. Zuo, X. Su, P. Zhang, J.A. Schlueter, M.E. Kelly and J.M. Williams, Phys. Rev. B **57** R5610 (1998); F. Zuo, J.A. Schlueter, M.E. Kelly and J.M. Williams, Phys. Rev. B **54**, 11973 (1996).
- [49] S. Belin, T. Shibauchi, K. Behnia and T. Tamegai, J. of Superconductivity, **12**, 497 (1999).

- [50] D. K. Finnemore, *Phenomenology and Applications of High Temperature Superconductors*, Addison Wesley, Reading MA (1992), pp. 164.
- [51] Y. Ando, G.S. Boebinger, A. Passner, L.F. Schneemeyer, T. Kimura, M. Okuya, S. Watauchi, J. Shimoyama, K. Kishio, K. Tamasaku, N. Ichikawa and S. Uchida, Phys. Rev. B **60**, 12475 (1999) and references therein.
- [52] A. Houghton, R. A. Pelcovits, and A. Sudbo, Phys. Rev. B, **40** (1989) 463.
- [53] See *e.g.* *Principles of the theory of solids*, (second edition) J.M. Ziman (Cambridge University Press, 1972) and references therein.
- [54] C.H. Mielke *et al.* to be published.
- [55] J. Singleton and C.H. Mielke, to be published (2001).
- [56] T. Sasaki, W. Biberacher, K. Neumaier, W. Hehn, K. Andres and T. Fukase, Phys. Rev. B. **57**, 10889 (1998).
- [57] M. Lang, F. Steglich, N. Toyota and T. Sasaki, Phys. Rev. B **49**, 15227 (1994).
- [58] S.L. Lee, F.L. Pratt, S.J. Blundell, C.M. Aegerter, P.A. Pattenden, K.H. Chow, E.M. Forgan, T. Sasaki, W. Hayes and H. Keller, Phys. Rev. Lett. **79**, 1563 (1997).
- [59] M. Mola, S. Hill, J.S. Brooks and J.S. Qualls, Phys. Rev. Lett. **86**, 2130 (2001).
- [60] H. Mayaffre, P. Wzietek, D. Jerome and S. Bazovskii, Phys. Rev. Lett. **76**, 4951 (1996).
- [61] See J.E. Graebner, R.C. Haddon, S.V. Chichester and S.H. Glarum, Phys. Rev. B **41**, 4808 (1990) and references therein.
- [62] A similar curvature in H_{c2} versus T data has been observed in artificially-constructed 2D superconductors (Mo-Ge films of thickness ~ 2 nm; the field was applied perpendicular to the 2D planes), suggesting that it is a generic property of 2D superconductors; see J.M. Graybeal and M.R. Beasley, Phys. Rev. B **29**, 4167 (1984).
- [63] W. E. Lawrence and S. Doniach, in E. Kanda (ed.) Proc. 12th Int. Conf. Low Temp. Phys. (Kyoto, 1970), pp. 361.
- [64] T. Nakamura, T. Komatsu, G. Saito, T. Osada, S. Kagoshima, N. Miura, K. Kato, Y. Maruyama and K. Oshima, J. Phys. Soc. Jpn., **62** 4373 (1993).
- [65] R. C. Morris, R. V. Coleman, and R. Bhandari, Phys. Rev. B **5**, 895 (1972).
- [66] This procedure was carried out using Equations 12, 13, and 14 in the limit $T \rightarrow 0$ [54]; see Section 5 for a discussion of some of the difficulties inherent in this procedure.
- [67] *Superconductivity*, edited by R.D. Parks (Marcel Dekker, New York, 1969).
- [68] A number of authors have compared the magnetic-field orientation dependence of H_{c2} in organic superconductors with various theoretical expressions. It is found that the Ginzberg-Landau-effective-mass expressions fit the data reasonably well for angles away from $\theta = 90^\circ$. However, close to in-plane magnetic fields ($\theta = 90^\circ$), mechanisms limited by spin (rather than orbital) effects take over, so that a simple ratio of the in-plane H_{c2} to the perpendicular H_{c2} is NOT a reliable guide to the relative sizes of the coherence lengths. This point is discussed at some length in Reference [1], in M.-S. Nam *et al.* J. Phys.: Condens. Matter, **11**, L477 (1999), Reference [35] and References cited in these papers. In Reference [54] these problematic orientations are deliberately avoided.
- [69] W.R. White, A. Kapitulnik and M.R. Beasley, Phys. Rev. Lett. **66**, 2826 (1991).
- [70] The majority of dimensional crossover studies employing artificial layered structures focus on the effect of an in-plane magnetic field, which is not relevant in the current context; see *e.g.* S.T. Ruggiero, T.W. Barbee and M.R. Beasley, Phys.Rev. Lett. **45**, 1299 (1980) and references therein.